Az egészséges szövetekben kialakuló sugárreakciók

A szövetek proliferatív szerveződése

hierarchikus
flexibilis

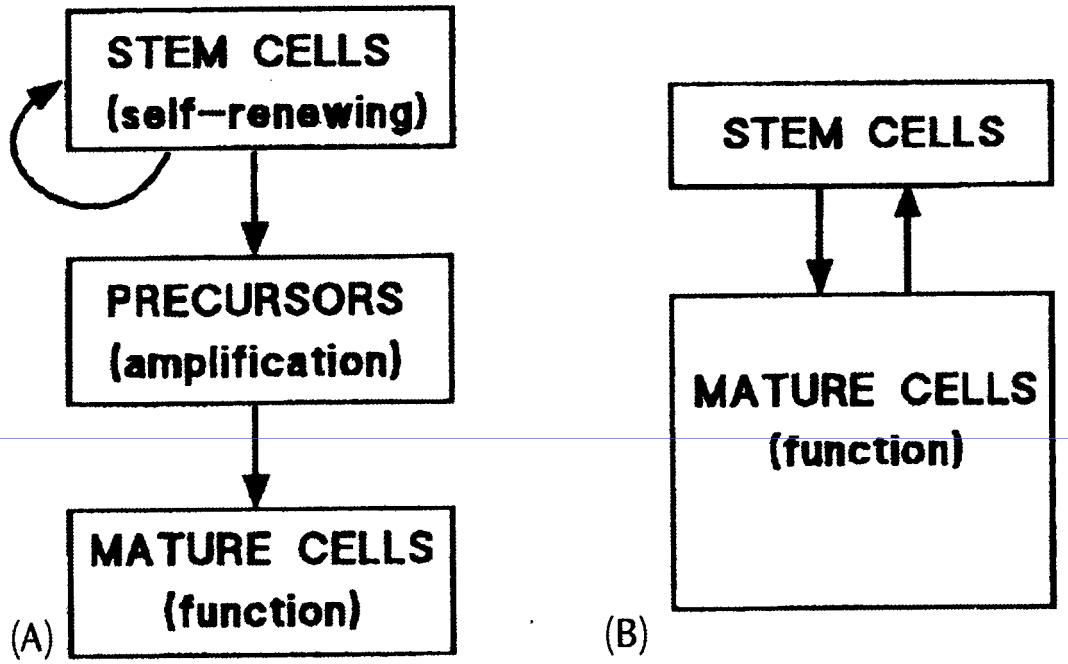

Figure 3.1 *Schematic outline of the proliferative organization of (A) hierarchical and (B) flexible normal-tissue systems.*

Normál szövetekben bekövetkező változások sugárhatásra

Korai és késői mellékhatások

A tünetek megjelenési ideje

Korai mellékhatások

A tünetek megjelenési idejét a dózis nem befolyásolja

A tünetek fennmaradási ideje dózis függő

Gyorsan proliferálódó szövetekben a tünetek hamarabb megjelennek

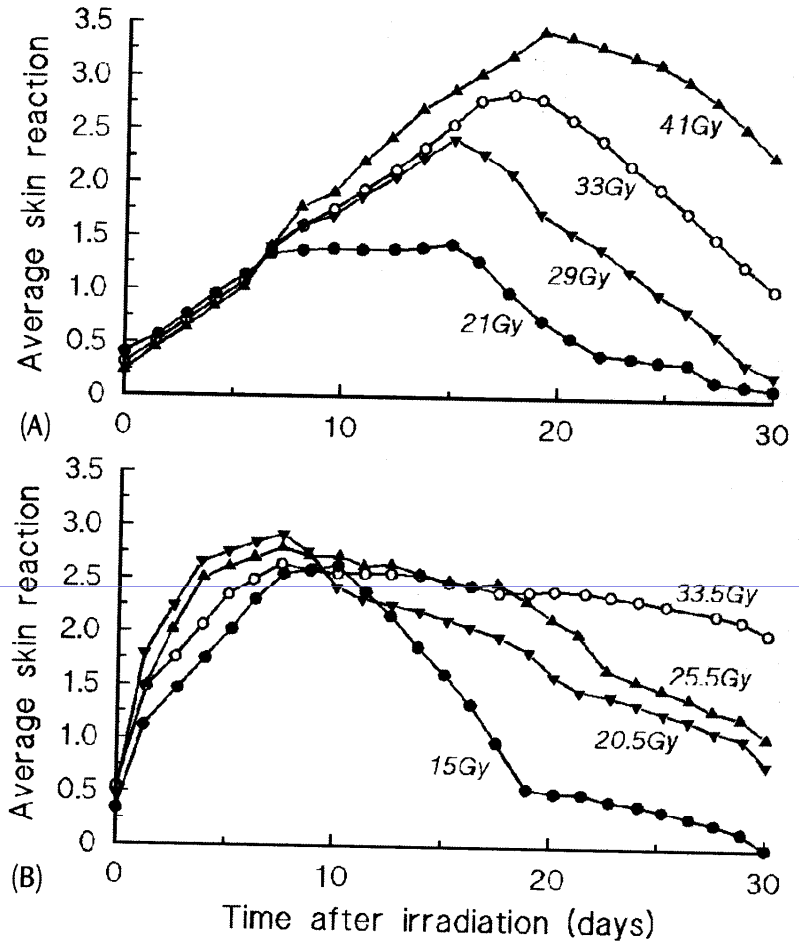

Figure 3.2 *The time-course of radiation-induced desquamation in the dorsal skin of the mouse foot: (A) normal skin; (B) plucked skin, showing a faster development of reactions due to a shorter cell cycle time. From Hegazy and Fowler (1973), with permission.*

Késői mellékhatások

A tünetek progrediálnak

A tünetek súlyosabbak korai látencia időnél

Konzekvenciális késői mellékhatások

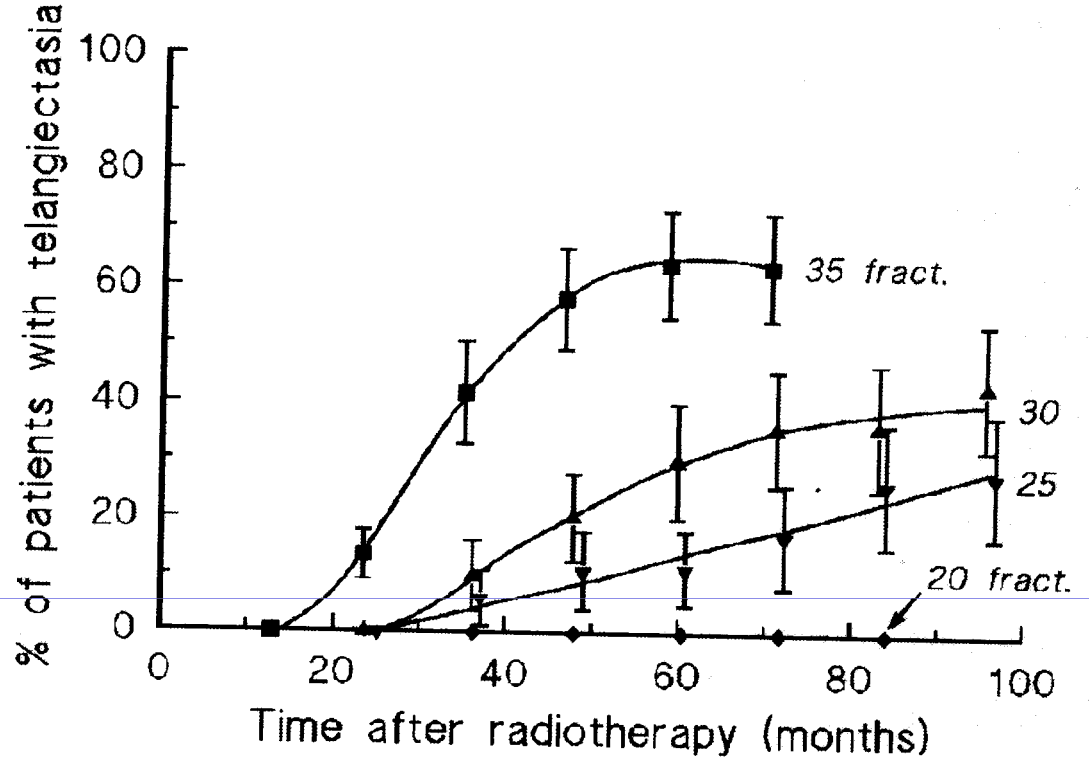

Figure 3.3 *The cumulative proportion of patients with distinct telangiectasia as a function of time after treatment with daily 2 Gy fractions. Note that telangiectasia develops more quickly after higher total doses and progresses over a number of years. From Turesson and Notter (1986), with permission.*

A tünetek látencia idejét nem a szerv sugárérzékenysége, hanem az érési sor ideje befolyásolja

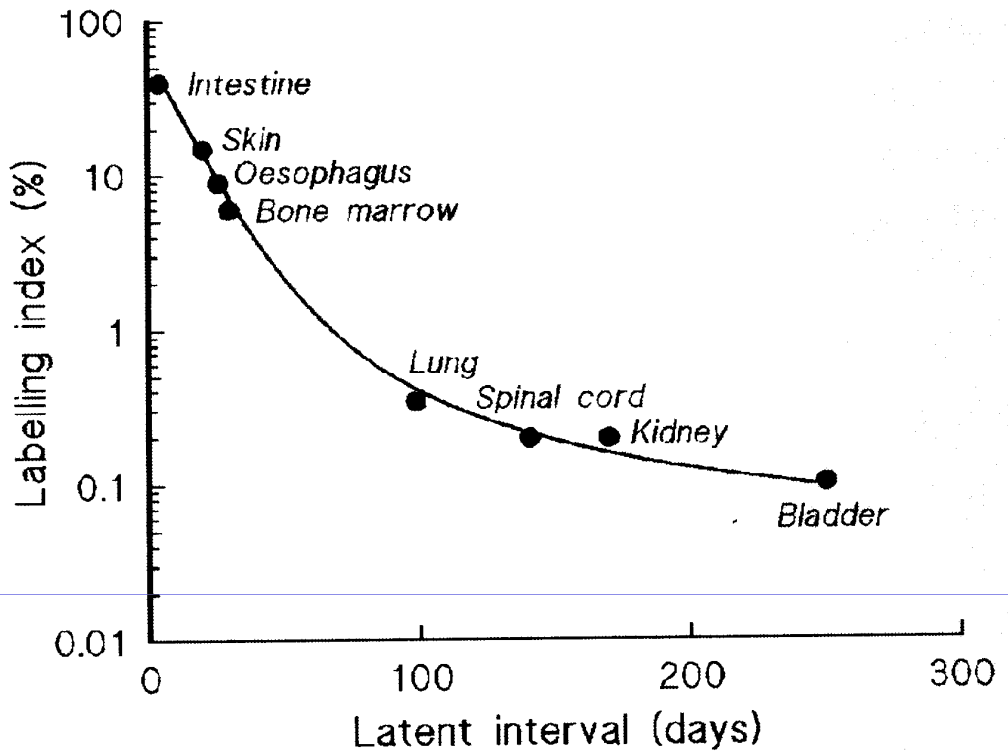

Figure 3.4 *Correlation of approximate latency times (for development of moderate to severe radiation-induced functional damage) with rate of proliferation (i.e. labelling index) in different rodent tissues. Rapidly proliferating tissues express their damage much earlier than slowly proliferating tissues. Data derived from various published sources.*

Sejtproliferációs változások besugárzás hatására

Table 3.1 *Cell turnover times and time of onset of compensatory proliferation in normal tissues*

Tissue	Cell turnover time (days)		Time of onset (days)	Authors
	Control	Stimulated		
Jejunum	0.6	0.4	3	Dewit *et al.* (1986)
Skin	4	1	8	Denekamp *et al.* (1976)
Lung	82	24	20/120	Coggle (1987)
Spinal cord	144	3	150	Zeman *et al.* (1964)
			20/120	Hornsey *et al.* (1981)
Kidney	144	11	120	Soranson and Denekamp (1986)
			90	Otsuka and Meistrich (1991)
Bladder	200	9	90–180	Stewart (1986)

The data in this table are approximate.

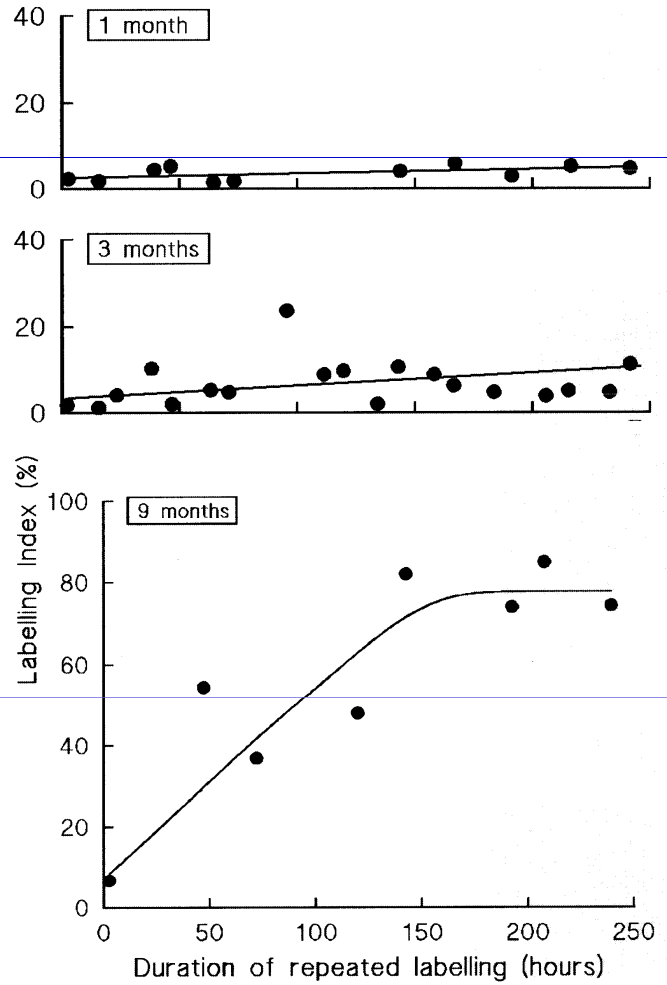

Figure 3.5 *Cell proliferation in the epithelium of the mouse bladder at 1, 3 and 9 months after irradiation with 25 Gy. The proliferation rate increased significantly from 3 months after irradiation but was not maximal until 9 months, coinciding with the histological appearance of hyperplasia and the occurrence of functional deficit. From Stewart (1986), with permission.*

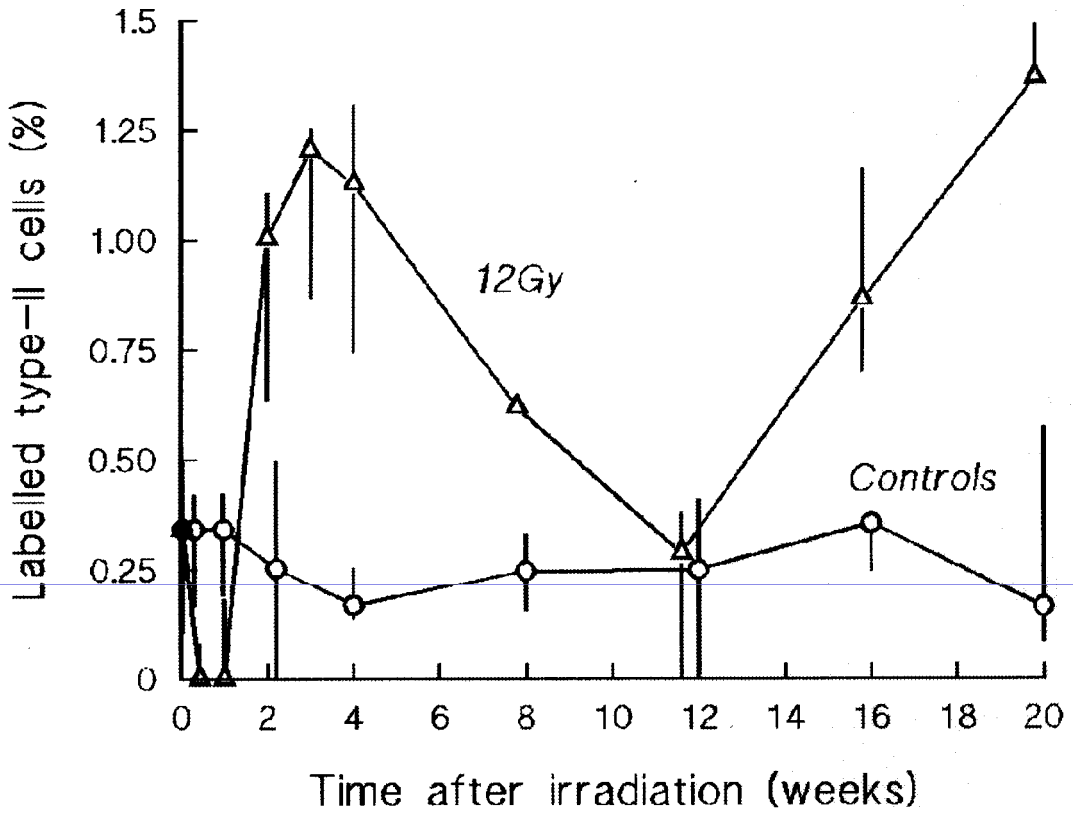

Figure 3.6 *Changes in the rate of proliferation in type-II pneumonocytes after thoracic irradiation of mice with 12 Gy, compared with unirradiated mice. From Coggle (1987) with permission.*

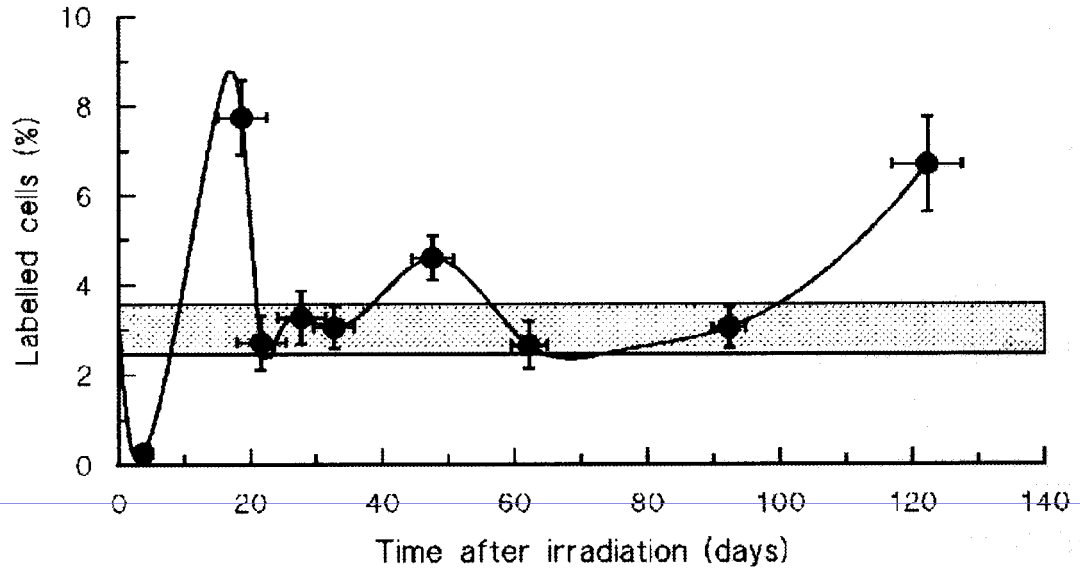

Figure 3.7 *Kinetics of glial-cell proliferation in the cervical spinal cord after a single dose of 20 Gy. In spite of the late onset of functional damage (5–6 months), an early wave of proliferation is observed. From Hornsey* et al. *(1981), with permission.*

Sugárreakciók egészséges szövetekben

Klonogén és funkcionális hatások

Bőr

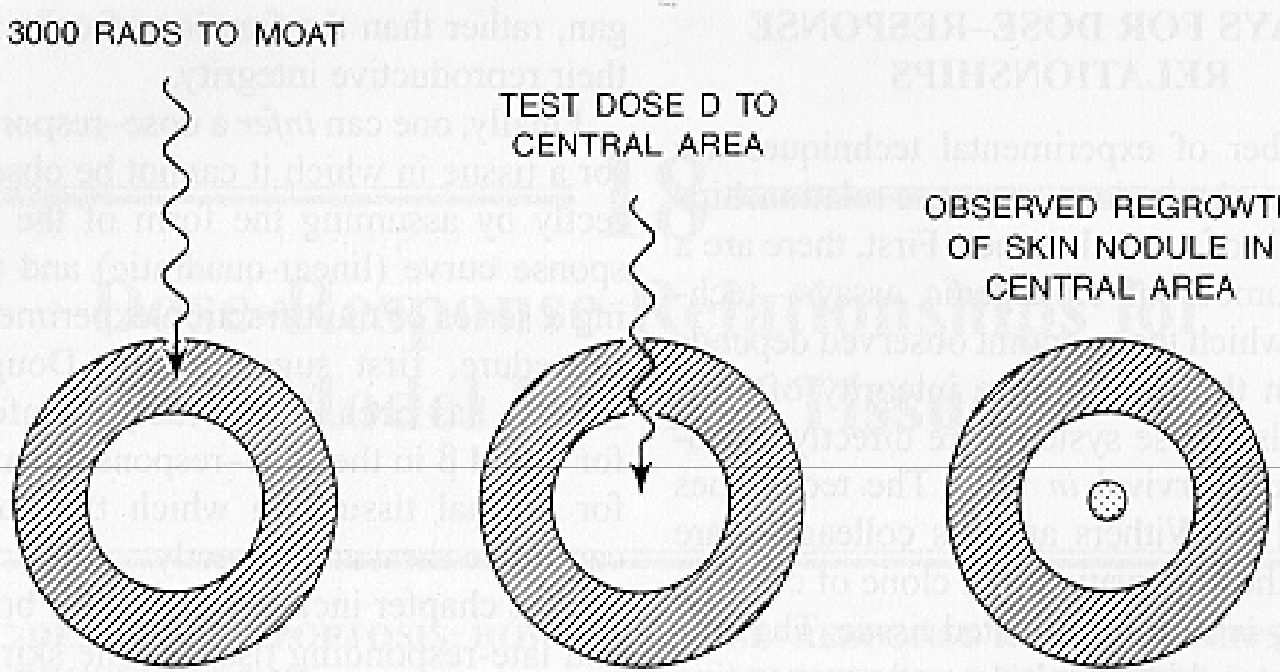

Figure 18.1. Technique used to isolate an area of skin for experimental irradiation. A superficial (30-kV) x-ray machine is used to irradiate an annulus of skin to a massive dose of about 3,000 rad (30 Gy). An isolated island of intact skin in the center of this "moat" is protected from the radiation by a metal sphere. The intact skin then is given a test dose (D) and observed for nodules of regrowing skin. (Adapted from Withers HR: Br J Radiol 40:187, 1967, with permission.)

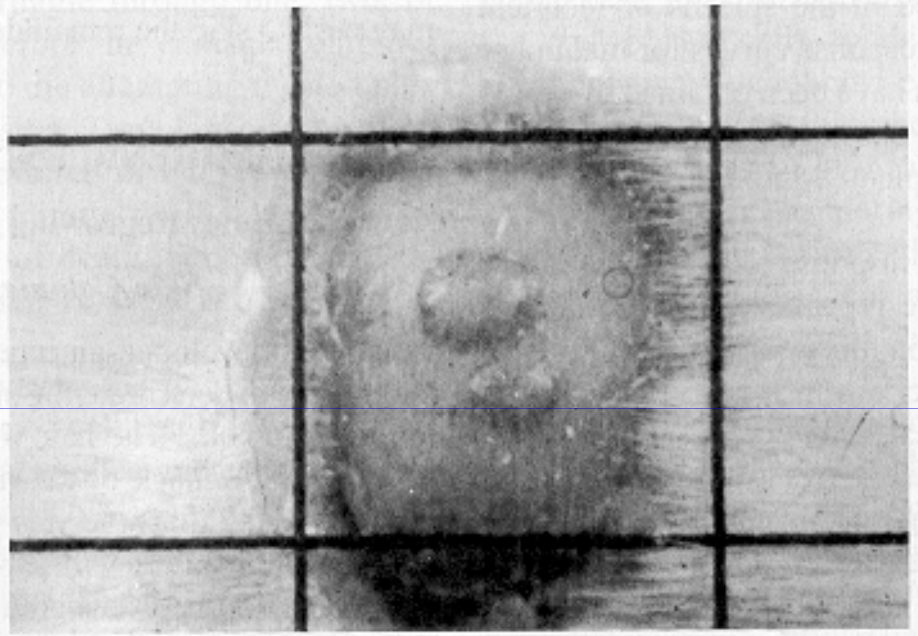

Figure 18.2. Photograph of a nodule of mouse skin regrowing from a single surviving cell in the treated area. (Courtesy of Dr. H. R. Withers)

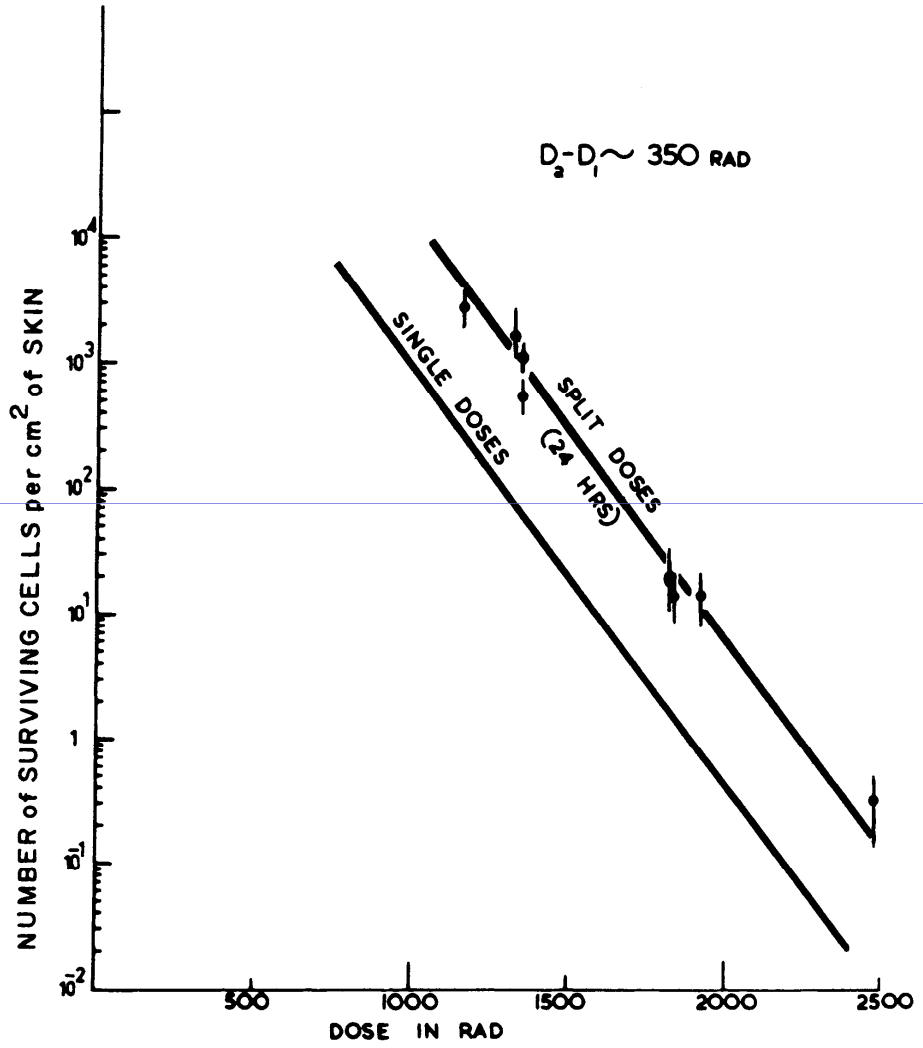

Figure 18.3. Single-dose and two-dose survival curves for epithelial cells of mouse skin exposed to 29-kVp x-rays. The 37% dose slope (D_0) is 1.35 Gy (135 rad). The ordinate is not the surviving fraction, as in the survival curves for cells cultured *in vitro*, but is the number of surviving cells per square centimeter of skin. In the two-dose survival curve the interval between dose fractions was always 24 hours. The curves are parallel, their horizontal separation being equal to 3.5 Gy (350 rad); this corresponds to D_q. From a knowledge of D_q and the slope of the survival curve, D_0, the extrapolation number, n, may be calculated. (From Withers HR: Radiat Res 32:227, 1967; and Withers HR: Br J Radiol 40:187, 1967, with permission.)

Bőr

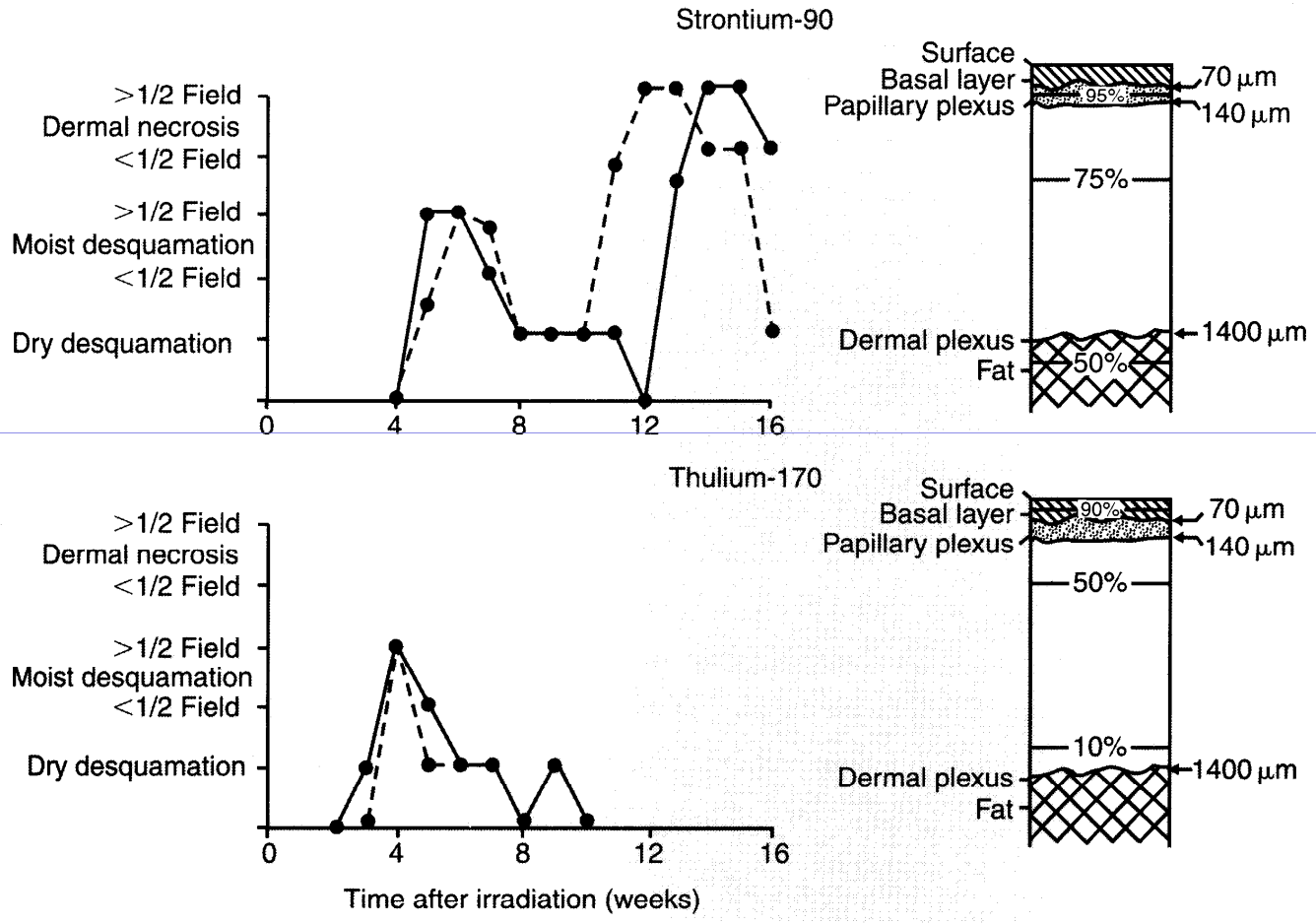

Figure 4.1 *Time-course of epithelial and dermal reactions in pig skin irradiated with single surface doses of 40 Gy ^{90}Sr or 130 Gy ^{170}Tm (solid and broken lines show results on two individual skin fields). The marked difference in radiation response is due to the greater penetration of ^{90}Sr emission into the dermis. From Hopewell (1986), with permission.*

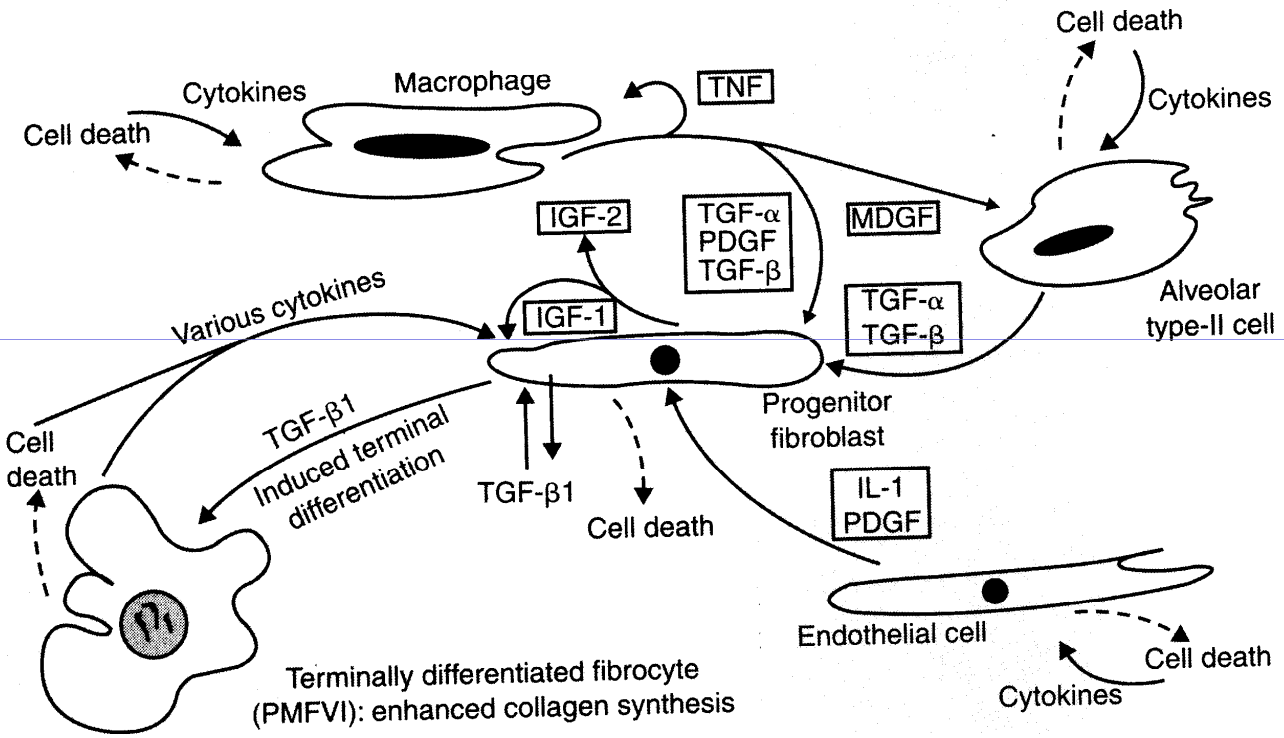

Figure 4.2 *Possible cellular interactions and events after irradiation of lung tissue. Modified from Rodemann and Bamberg (1995), with permission.*

Mucosa

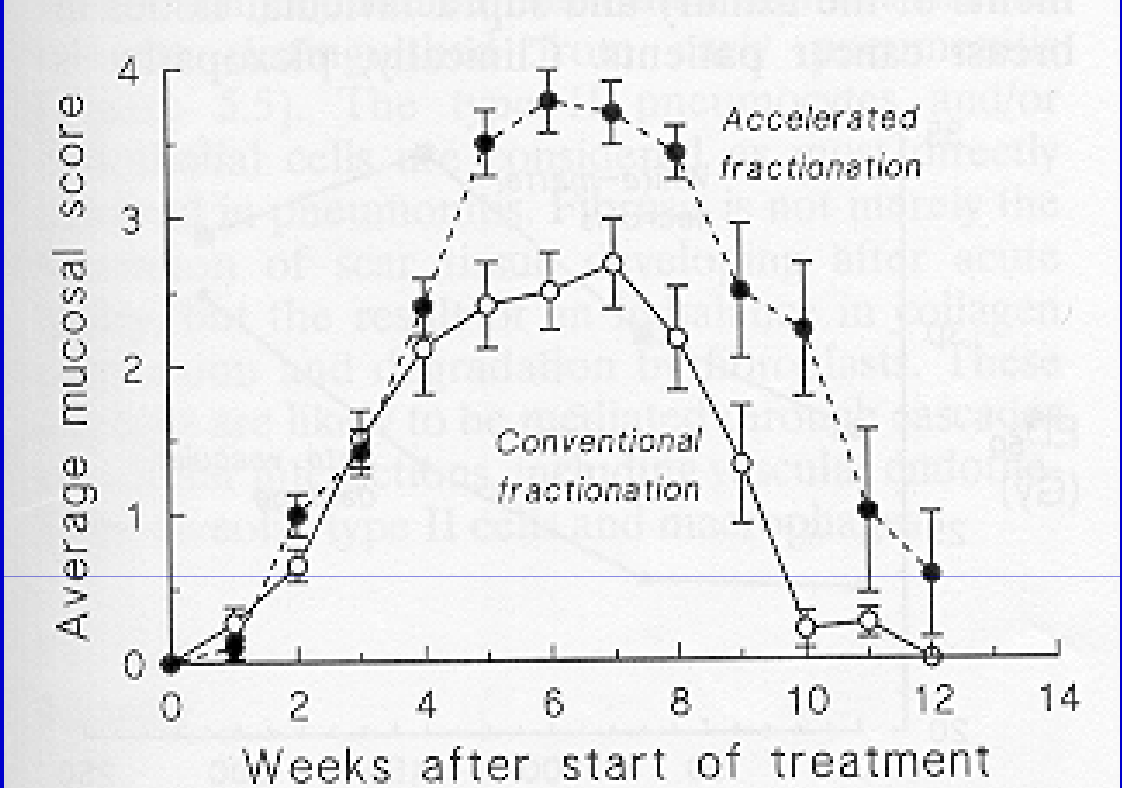

Figure 5.2 Time-course of mucosal reactions in patients treated with conventional daily fractionation or an accelerated schedule, concomitant-boost type (fractions/day for last 7–8 treatment days) to a dose of 68–70 Gy. Score 4 is fully confluent mucositis. From Kaanders *et al* (1992), with permission.

Vékonybél

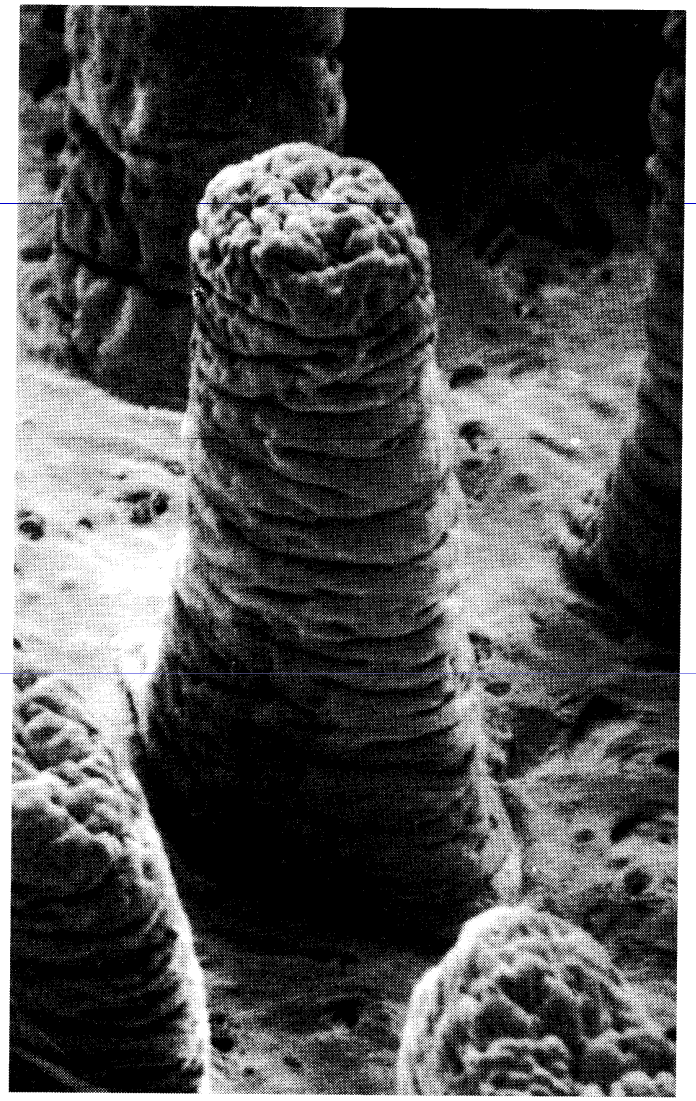

Figure 18.4. Scanning electron micrograph that allows three-dimensional visualization of the jejunal villi from the hamster. (Magnification × 175.) (From Taylor AB, Anderson JH: Micron 3:430–453, 1972, with permission.)

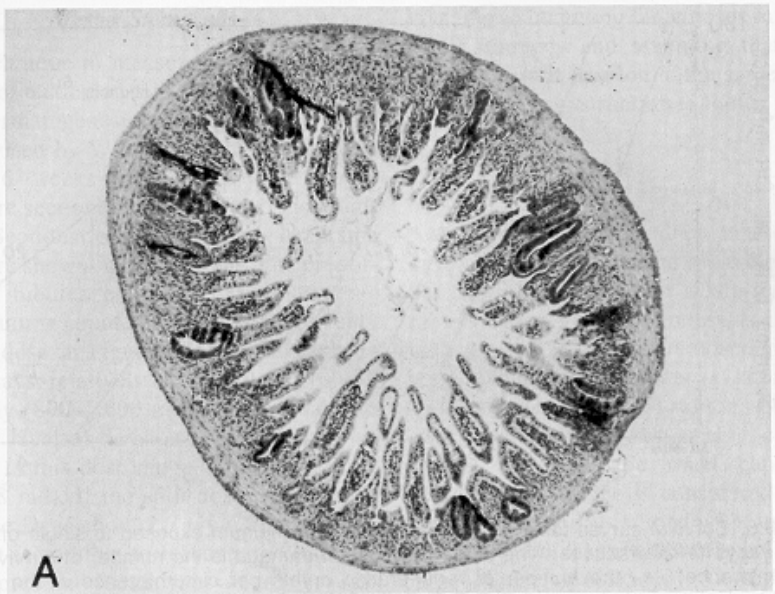

Figure 18.5. **A:** Section of mouse jejunum taken 3.5 days after a total-body dose in excess of 10 Gy. Note the shortened villi and the regenerating crypts. **B:** Regenerating crypts shown at a higher magnification. (From Withers HR: Cancer 28:78–81, 1971, with permission.)

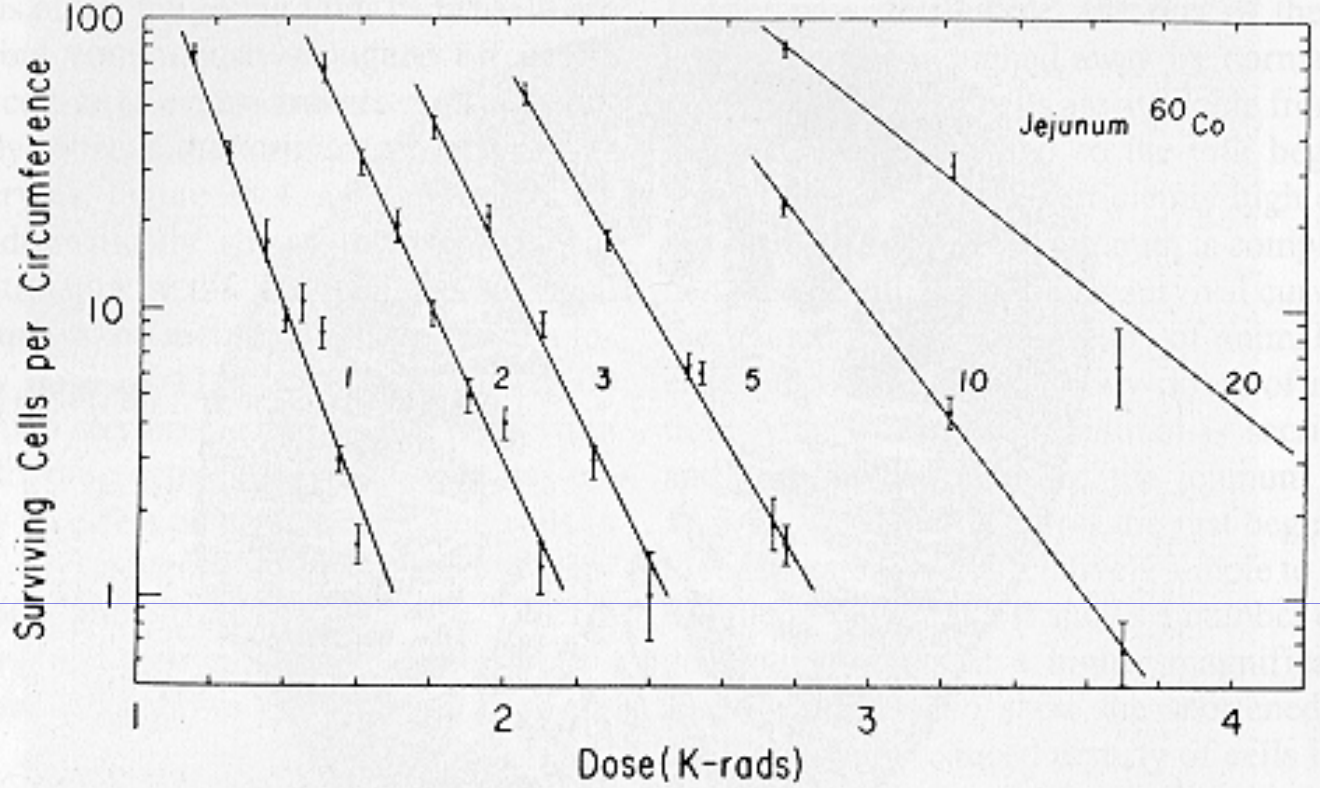

Figure 18.6. Survival curves for crypt cells in the mouse jejunum exposed to single or multiple doses of γ-rays (1–20 fractions). The score of radiation damage is the number of surviving cells per circumference (*i.e.*, the number of regenerating crypts per circumference of the jejunum) counted from sections such as those shown in Figure 18.5. This quantity is plotted on a logarithmic scale against radiation dose on a linear scale. The D_0 for the single-dose survival curve is about 1.3 Gy (130 rad). The shoulder of the survival curve is very large. The separation between the single- and two-dose survival curves indicates that the D_q is 4 to 4.5 Gy (400–450 rad). (From Withers HR, Mason K, Reid BO, et al.: Cancer 34:39–47, 1974, with permission.)

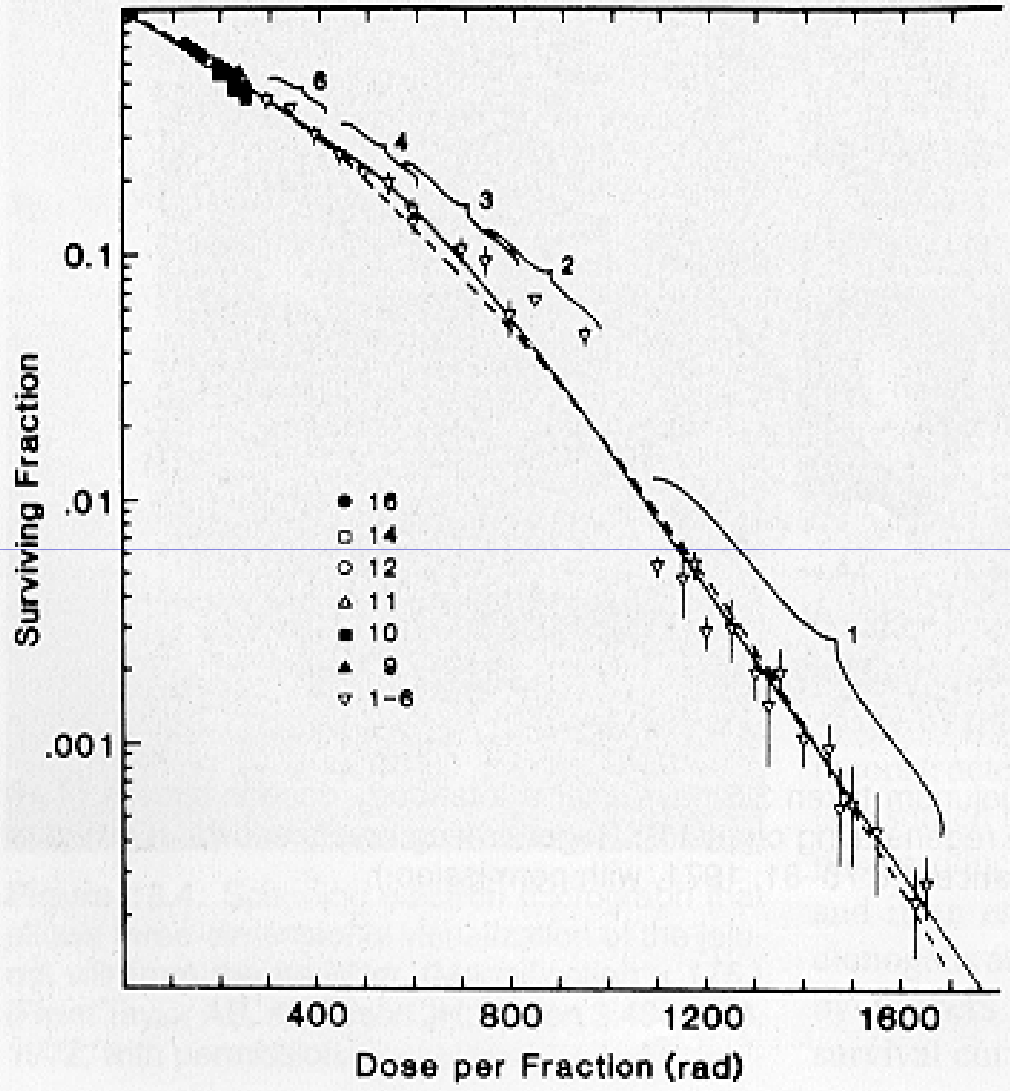

Figure 18.7. Effective single-dose survival curve reconstructed from multifraction experiments for clonogenic cells of the jejunal crypts of mice. The numbers on the curve refer to the number of fractions used to reconstruct that part of the curve. The initial and final slopes are about 3.57 and 1.43 Gy (357 and 143 rad), respectively. The quasithreshold dose is 4.3 Gy (430 rad). The data are equally well fitted by the linear-quadratic formulation. (From Thames HD, Withers R, Mason KA, Reid BO: Dose survival characteristics of mouse jejunal crypt cells. Int J Radiat Oncol Biol Phys 7:1591–1597, 1981, with permission.)

Vese

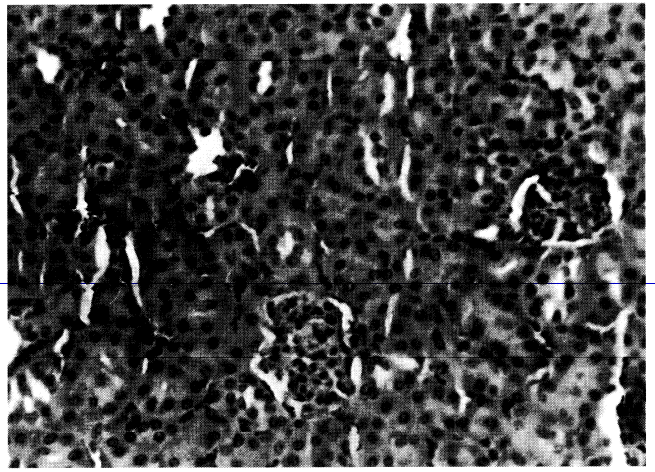

A

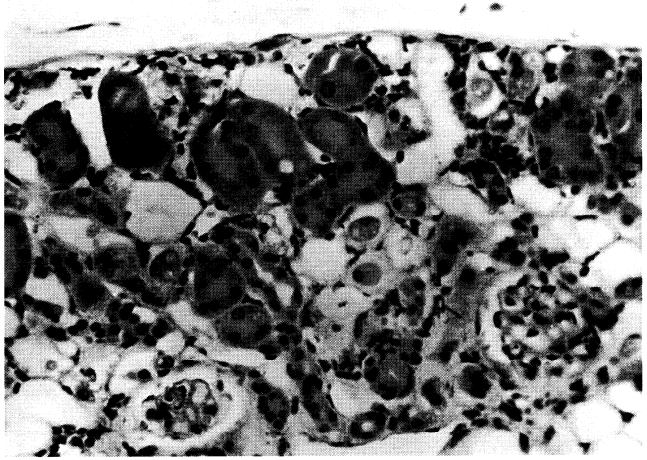

B

Figure 18.11. Photomicrographs of mouse kidney. **A:** Normal, showing proximal tubules in contact with capsule. (Hematoxylin–eosin stain, magnification ×400) **B:** Sixty weeks after 13 Gy (1,300 rad). Note normal proximal tubules and glomeruli amid ghosts of deepithelialized tubules. One epithelialized tubule is in contact with capsule. (Hematoxylin–eosin stain, magnification ×200) (From Withers HR, Mason KA, Thames HD: Late radiation response of kidney assayed by tubule cell survival. Br J Radiol 59:587–595, 1986, with permission.)

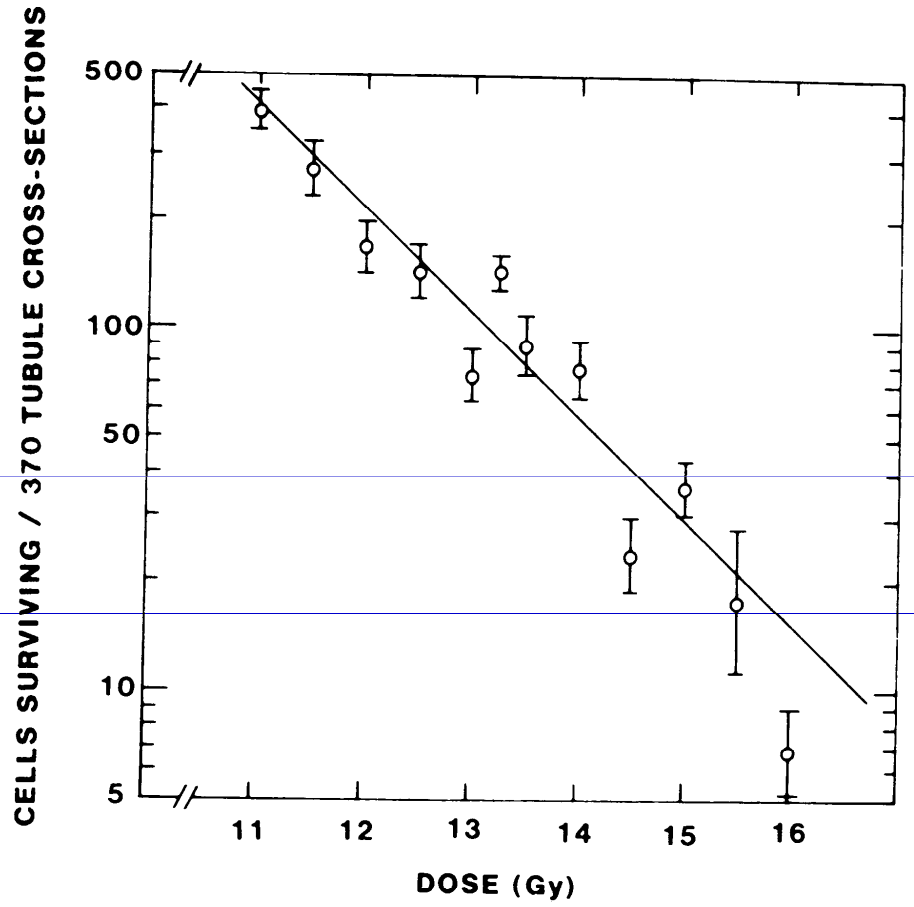

Figure 18.12. Dose–survival curve for tubule-regenerating cells. The D_0 is 1.53 Gy (153 rad). (From Withers HR, Mason KA, Thames HD Jr: Br J Radiol 59:587–595, 1986)

Központi idegrendszer és gerincvelő

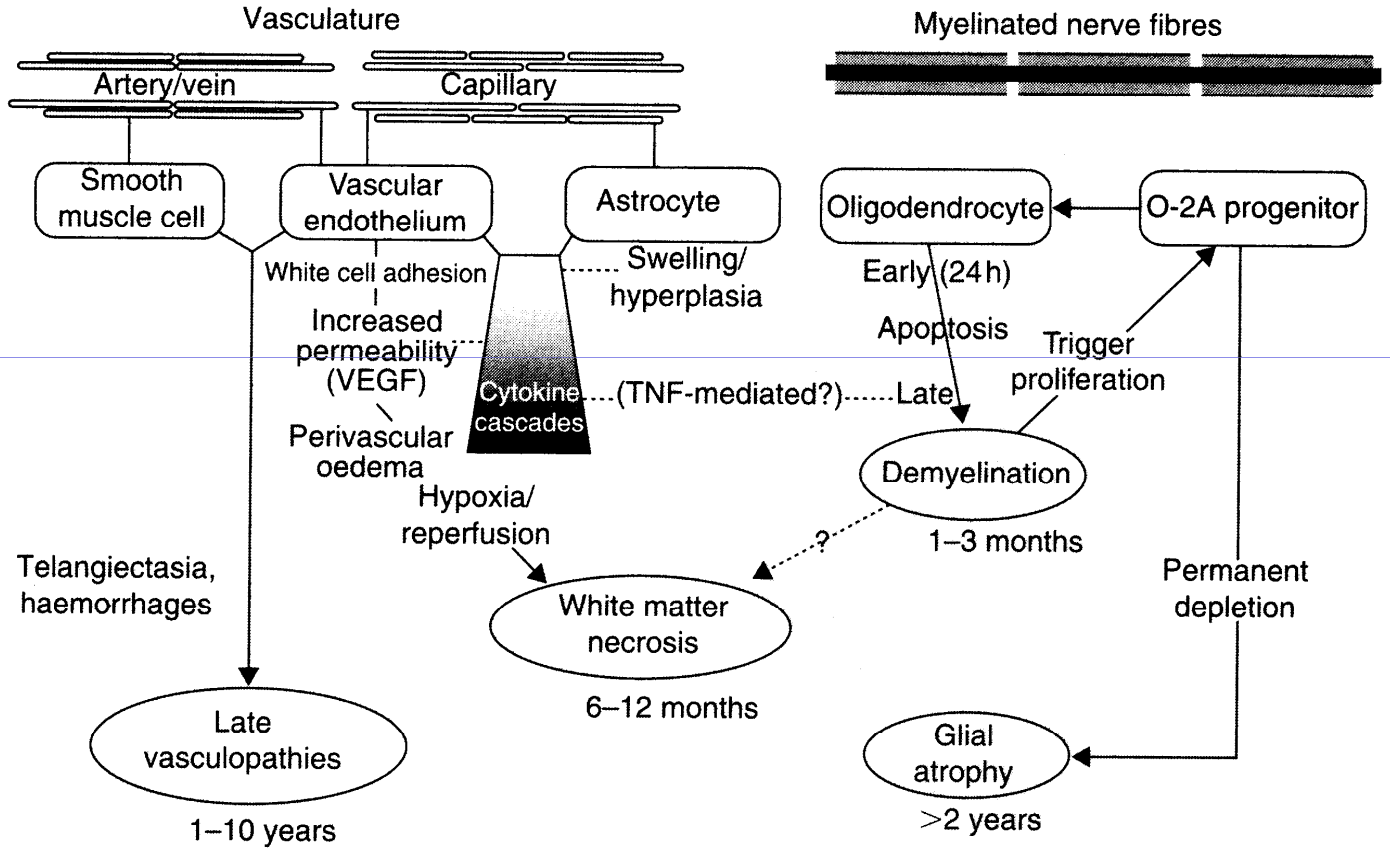

Figure 4.4 *Schematic outline of tissue components and cell types and their potential role in the pathophysiology of radiation-induced lesions in the central nervous system.*

Gerincvelő

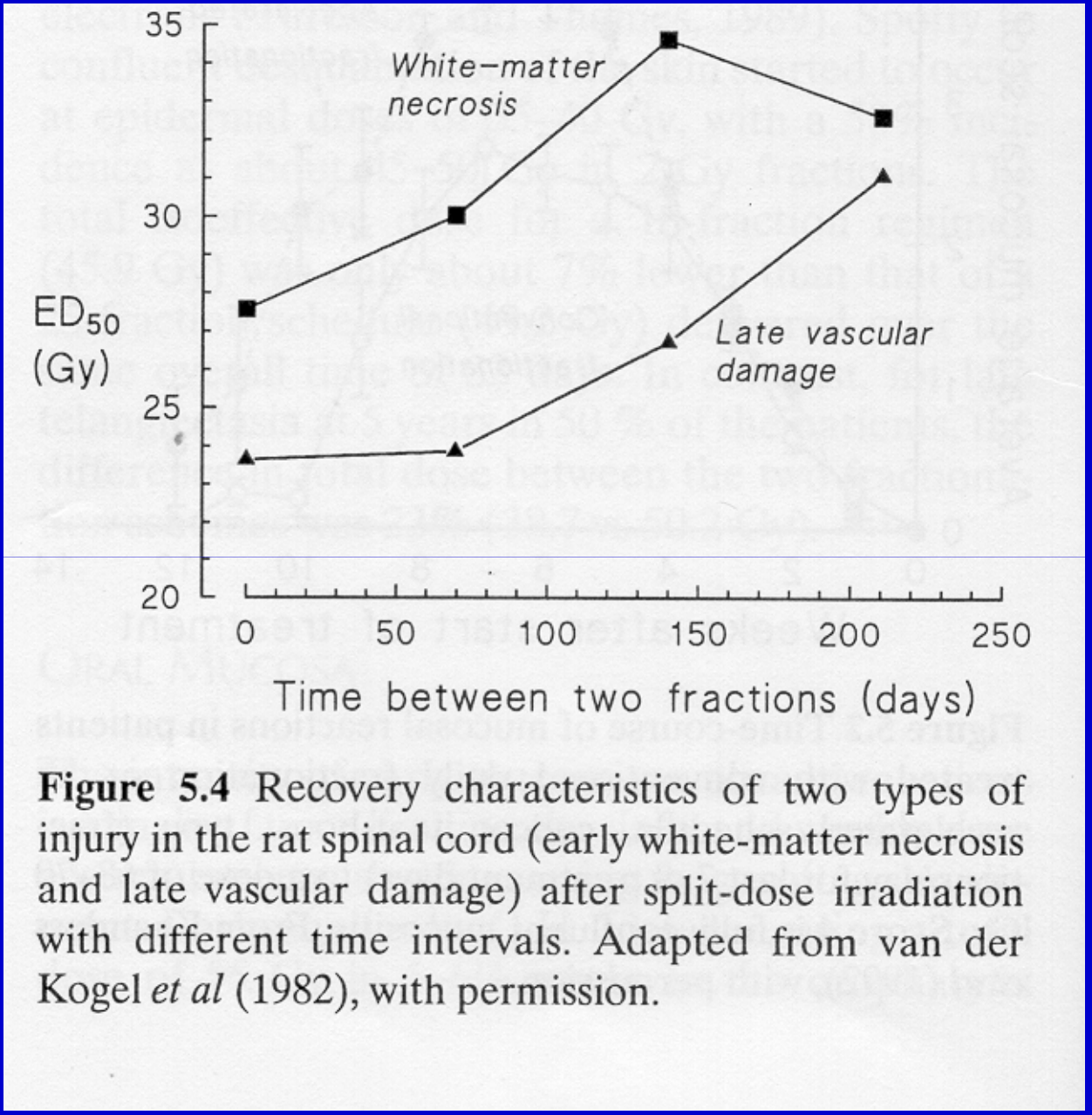

Figure 5.4 Recovery characteristics of two types of injury in the rat spinal cord (early white-matter necrosis and late vascular damage) after split-dose irradiation with different time intervals. Adapted from van der Kogel *et al* (1982), with permission.

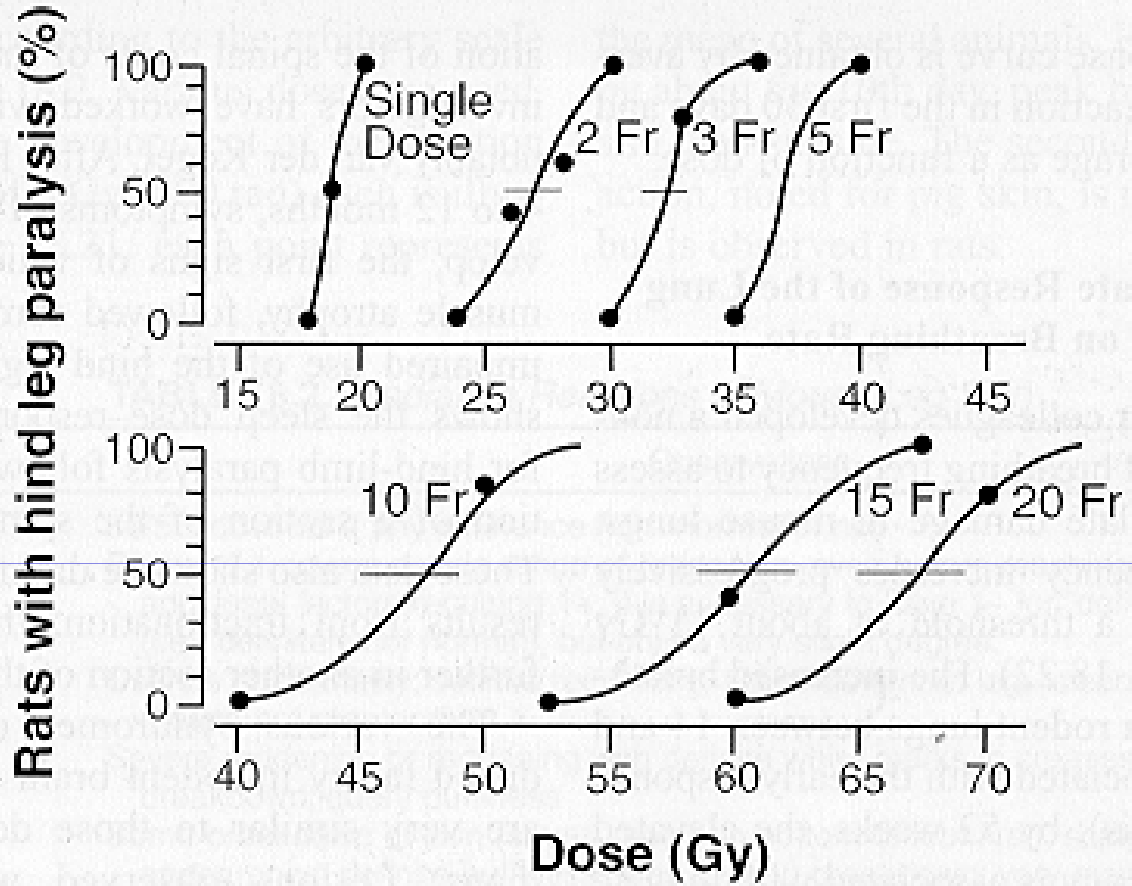

Figure 18.23. Dose–response curves for the induction of hind-leg paralysis in rats following irradiation of a section of the spinal cord (L2–L5). Note how the dose necessary to produce paralysis increases rapidly with increasing number of fractions. (Redrawn from van der Kogel AJ: Late Effects of Radiation on the Spinal Cord, pp 1-160. Rijswik, The Netherlands, The Radiobiological Institute of The Organization for Health Research TNO, 1979, with permission.)

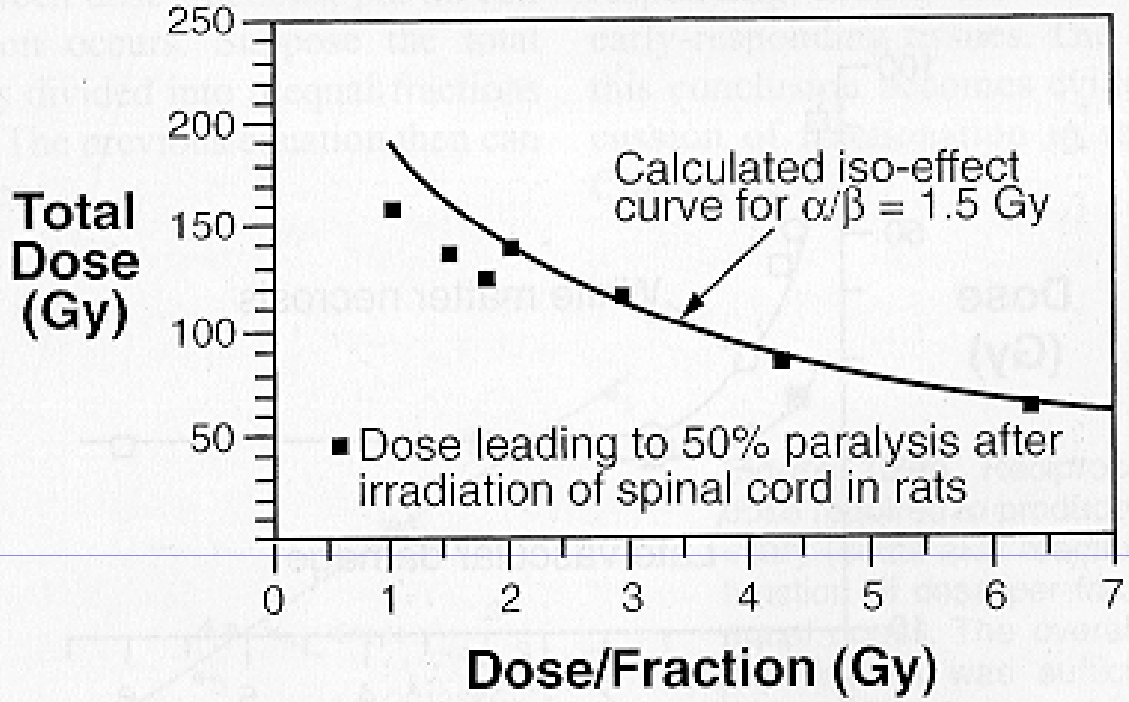

Figure 18.24. The data points show total dose, as a function of dose per fraction, to produce paralysis in 50% of rats after irradiation of the spinal cord. The curve is an isoeffect relationship based on the linear-quadratic equation with an α/β of 1.5 Gy. The experimental data suggest that the linear-quadratic model overestimates tolerance for dose per fraction values less than 2 Gy. This may be a result of incomplete repair, because the interfraction interval was only 4 hours. (Adapted from van der Kogel AJ: Central nervous system radiation injury in small animal models. In Gutin PH, Leibel SA, Sheline GE [eds]: Radiation Injury to the Nervous System, pp 91–112. New York, Raven Press, 1991, with permission.)

Tüdő

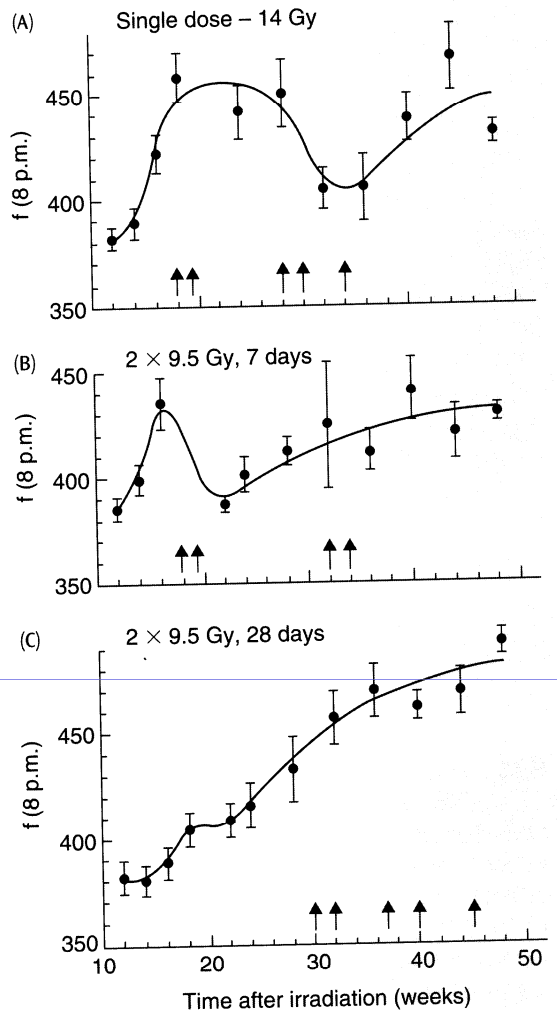

Figure 4.5 *Evidence for two phases of radiation response in the mouse lung. Using breathing rate as a measure of damage, two waves of response are seen after single doses (panel A). (B, C) Split-dose irradiation, especially with a gap of 28 days, reduced the severity of the first phase (acute pneumonitis), but had little effect on the second phase (fibrosis). Arrows indicate the death of individual mice. From Travis and Down (1981), with permission.*

Table 4.1 *Normal-tissue tolerance doses and α/β values*

Tissue	End-point	Risk (%)	Dose* (Gy)	α/β ratio (Gy)
Skin	Desquamation	50	55–60	10–12
	Fibrosis	5	60–65	2–3
	Telangiectasia	50	55–60	3–4
Oral mucosa	Confluent mucositis	50	65–70	~10
Small intestine	Late fibrosis, fistulae	5	50	3–4
Colon, rectum	Late fibrosis, fistulae	5	60	3–4
Brain, spinal cord	Necrosis	<1	50	2
		5	60	
Nerve plexus	Demyelination, fibrosis	5	65	3–4
Lung	Pneumonitis	5	20**	2–4
Heart	Pericarditis	<5	35–40	2–3
	Pericarditis	50	50–60	
	Cardiomyopathy	15–20	30–36	
	Ischaemic heart disease	<5	30	
Kidney	Glomerulosclerosis	<5	20**	2–3
Liver	Hepatitis, VOD	5	25–30**	3
Bladder	Cystitis, ulcers	<5	60–65	5–10

* Delivered as 2 Gy per fraction.
** Whole organ irradiated, partial volume tolerance usually much higher; VOD, veno-occlusive disease.
The tolerance doses and associated risks should be considered as approximations, and only for conventional daily fractionation with fraction doses of 2 Gy of high-energy photons. Irradiated volumes are generally large, and tolerance doses may increase with volume reduction, but the volume effect is widely different for different organs (see Chapter 5).

A besugárzott térfogat hatása

Szöveti szerveződés

soros
párhuzamos elrendeződés

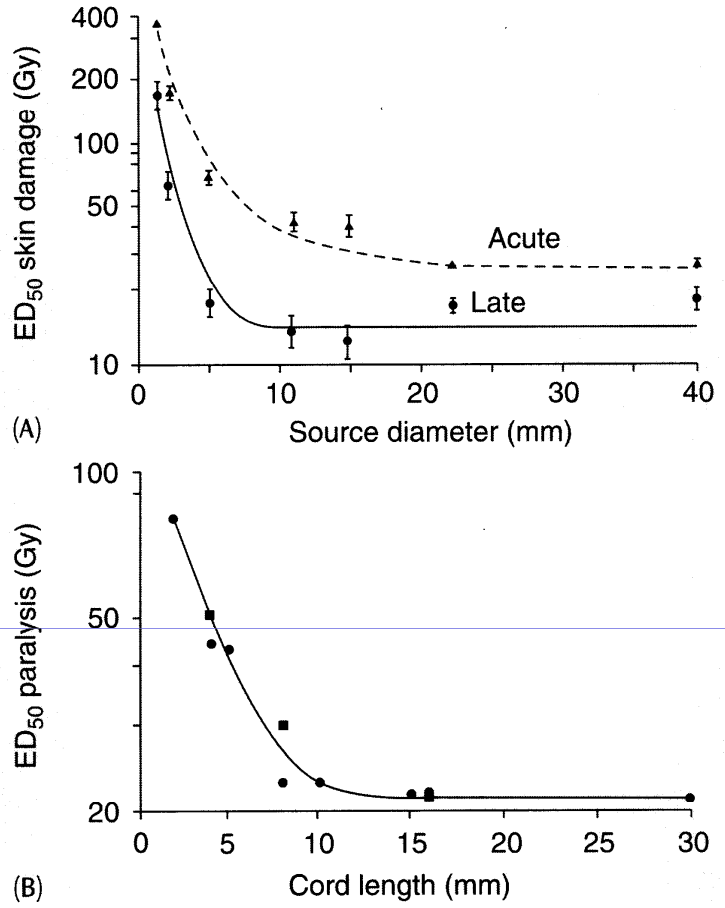

Figure 5.1 *The influence of field-size on biological response in pig skin (A) and rat spinal cord (B) after single-dose irradiation with small fields. In each case there is a steep rise in ED_{50} as field-size is reduced below 10 mm, with very little change in ED_{50} for larger field-sizes. From Hopewell and Trott (2000), with permission.*

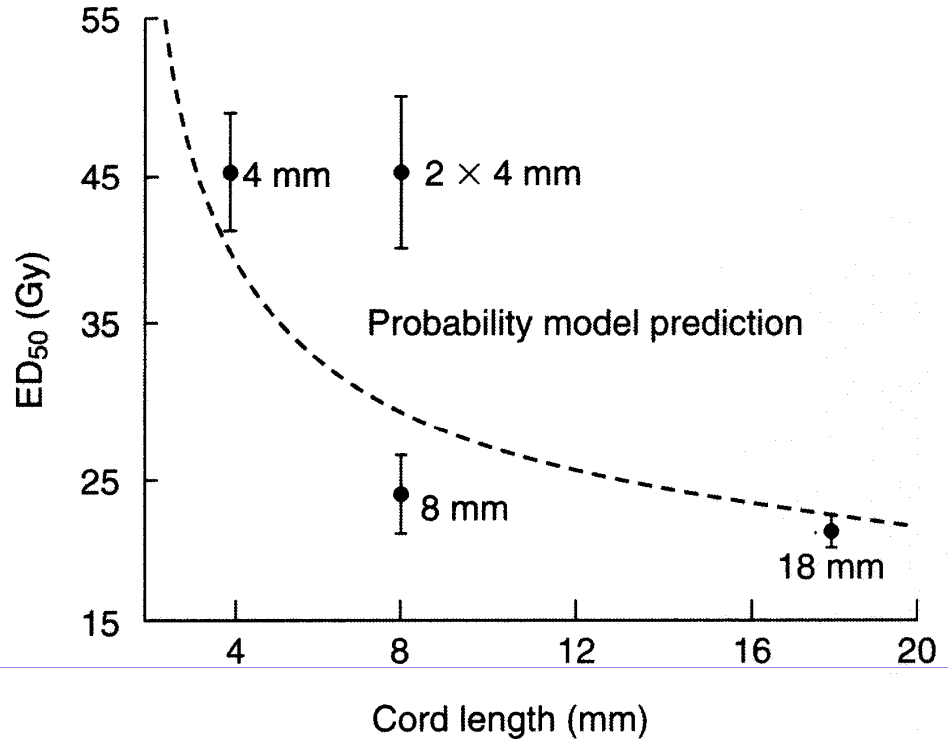

Figure 5.2 *For cord lengths below 10 mm, field-size rather than total volume determines the response of rat cervical spinal cord. The single fields (4, 8, 18 mm) were centred around C5, the two concomitant 4 mm fields were at C1/2 and C7/T1, separated by ~10 mm. Data show the ED_{50} for induction of white-matter necrosis. Statistical models predict a continuously rising curve as shown. Unpublished results, AJ van der Kogel.*

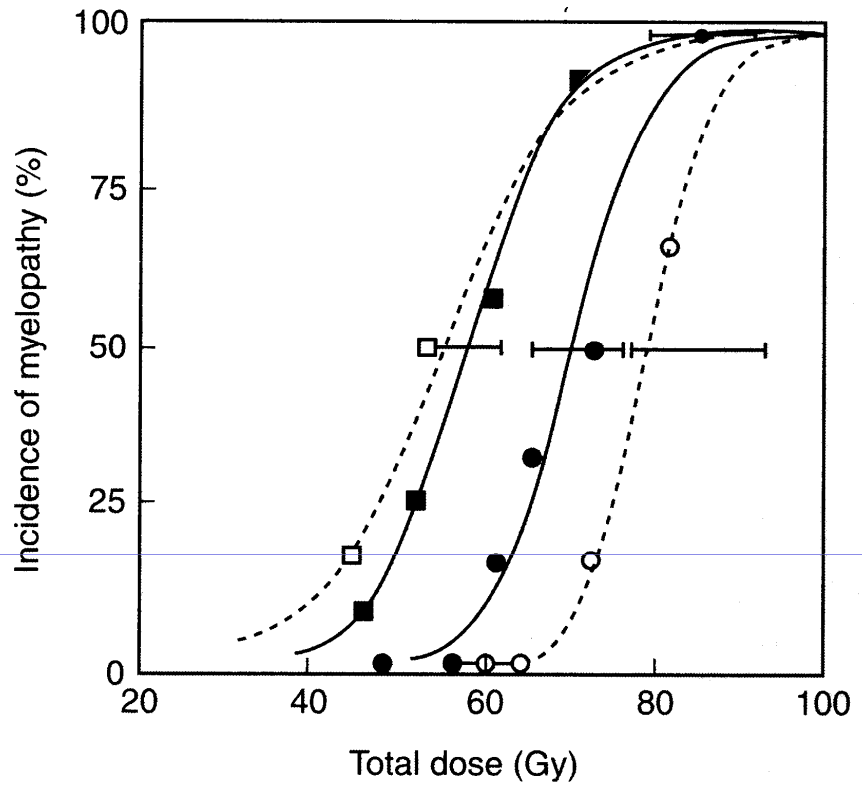

Figure 5.3 *Influence of change in field-size on spinal cord damage in dogs. Increasing the field-size from 4 cm (circles) to 20 cm (squares) had a more marked influence on the development of neurological signs of injury (dotted lines) than on the occurrence of severe pathological lesions (solid lines). Redrawn from Powers* et al. *(1998), with permission.*

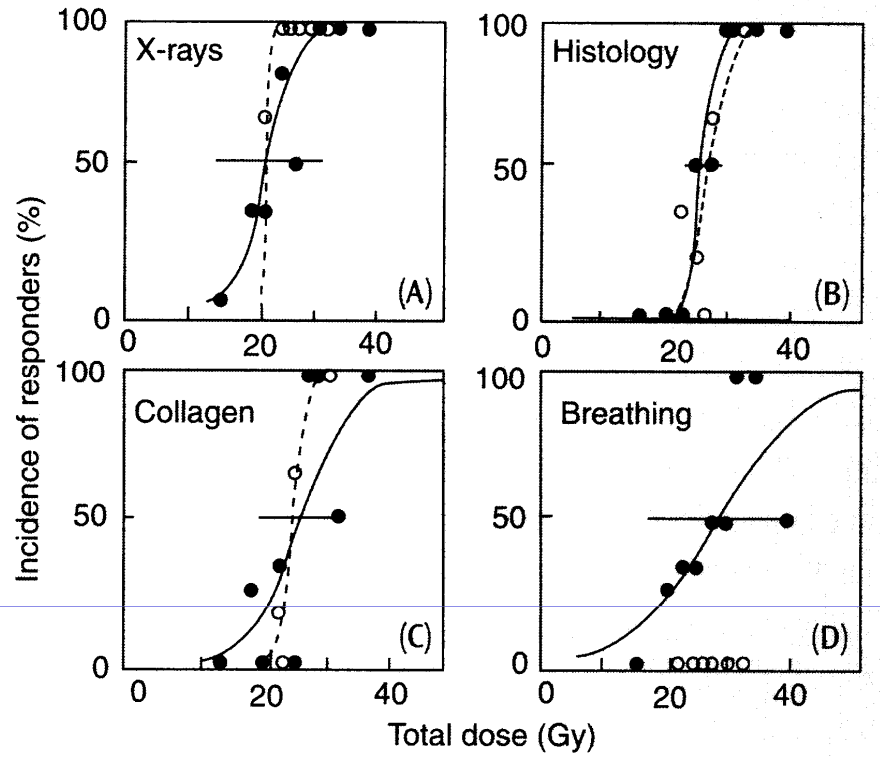

Figure 5.4 *Dose–response curves for radiation-induced lung damage in pigs after irradiation with five fractions, given to half of the right lung (○) or to the whole right lung (●). Damage was assessed from radiographic changes (A), histological evidence of fibrosis (B), elevated hydroxyproline (collagen) levels (C), or increased breathing rate (D). Only the functional end-point demonstrated a volume effect. From Herrmann* et al. *(1997), with permission.*

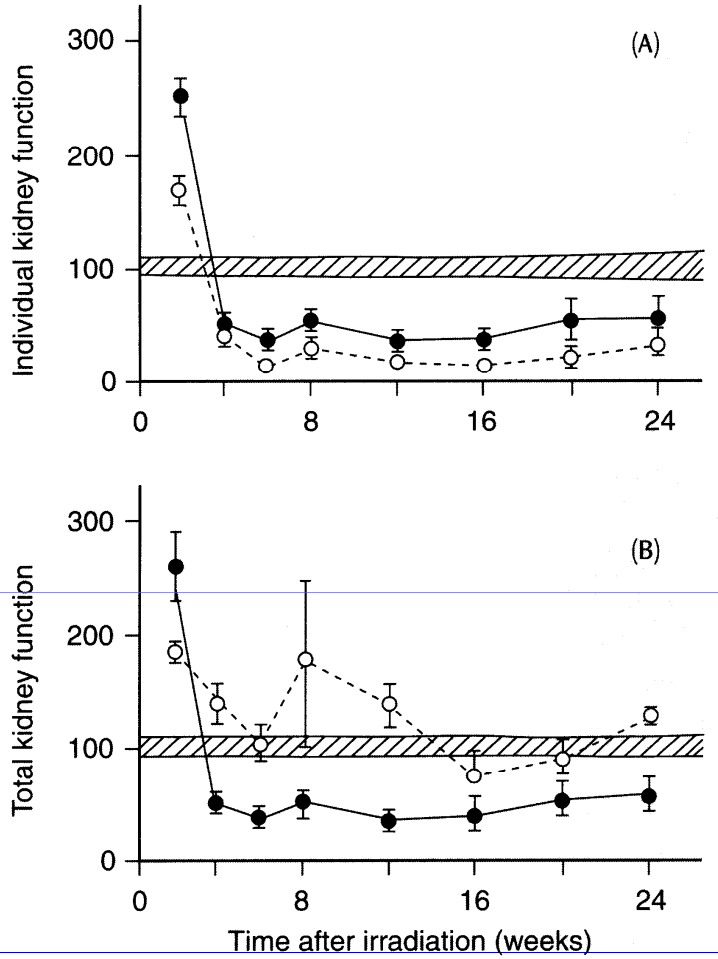

Figure 5.5 *Time-related changes in glomerular filtration rate in pigs in which one (○) or both (●) kidneys were irradiated with a single dose of 12.6 Gy. Panel A shows the change in individual kidney function, as a percentage of control values, and panel B shows the total renal function in the same pigs. Redrawn from Robbins and Hopewell (1988).*

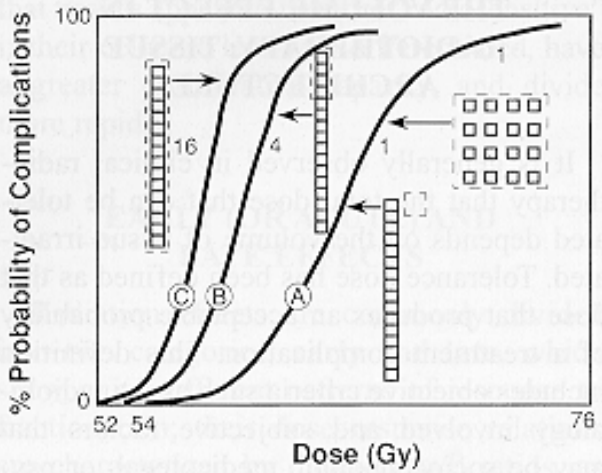

Figure 19.1. Relationship between dose and probability of complications for different types of normal tissues. Curve A relates to a normal tissue in which the functional subunits are not arranged serially regardless of whether one or all subunits are exposed (*i.e.*, regardless of field size). It also applies to a normal tissue in which functional subunits are arranged serially if only one subunit is exposed (*i.e.*, if the field is small). Note that the curve is relatively shallow (*i.e.*, the probability of a complication rises relatively slowly with dose). Curves B and C refer to a tissue with serially arranged functional subunits; the complication curve gets steeper and moves to lower doses as the treatment field size increases. For example, curves B and C relate to 4 or 16 functional subunits exposed. (Note that the position of the curves in relation to the abscissae is arbitrary, resulting from two assumptions: an effective D_0 of 4 Gy for a survival curve for cells exposed to multiple doses of 2 Gy, and that 58 Gy in 2-Gy fractions sterilizes 10% of the functional subunits.) (Adapted from Withers HR, Taylor JMG, Maciejewski B: Treatment volume and tissue tolerance. Int J Radiat Oncol Biol Phys 14:751–759, 1988, with permission.)

TABLE 19.2. *A Compilation of Tissue and Organ Sensitivities*

	Injury	$TD_{5/5}$, Gy	$TD_{50/5}$ Gy	Field Size
Class I organs				
Bone marrow	Aplasia, pancytopenia	2.5	4.5	Whole segment
Liver	Acute and chronic hepatitis	30	40	Whole
		50	55	1/3
Intestine	Obstruction, perforation, fistula	40	55	Whole
		50	65	1/3 or 1/2
Stomach	Perforation, ulcer, hemorrhage	50	65	Whole
		60	70	1/3
Brain	Infarction, necrosis	45	60	Whole
		60	75	1/3
Spinal cord	Infarction, necrosis	47	—	20 cm
		50	70	5 or 10 cm
Heart	Pericarditis and pancarditis	40	50	Whole
		60	70	1/3
Lung	Acute and chronic pneumonitis	17.5	24.5	Whole
		45	65	1/3
Kidney	Acute and chronic nephrosclerosis	23	28	Whole
		50	45	1/3 or 1/2
Class II organs				
Oral cavity and pharynx	Ulceration, mucositis	60	75	50 cm^2
Skin	Acute and chronic dermatitis, telangiectasia	55	65	100 cm^2
Esophagus	Esophagitis, ulceration	55	50	Whole
		60	70	1/3
Rectum	Ulcer, stenosis, fistula	60	80	no vol effect
Salivary glands	Xerostomia	32	46	1/3 or 1/2
Bladder	Contracture	65	80	2/3
		80	85	1/3
Ureters	Stricture	70	100	5–10 cm length
Testes	Sterilization	1	2	Whole
Ovaries	Sterilization	2–3	6–12	Whole (age dep.)
Growing cartilage, child bone	Growth arrest, dwarfing	10	30	Whole
Mature cartilage, adult bone	Necrosis, fracture, sclerosis	60	100	Whole
		60	100	10 cm^2
Eye				
Retina	Blindness	45	65	Whole
Cornea		50	6	Whole
Lens	Cataract	10	18	Whole
Endocrine				
Thyroid	Hypothyroidism	45	150	Whole
Adrenal	Hypoadrenalism	60		Whole
Pituitary	Hypopituitarism	45	200	Whole
Peripheral nerves	Neuritus	60	100	
Ear				
Middle	Serous otitis	30	40	No vol effect
Vestibular	Meniere's syndrome	60	70	
Class III organs				
Muscle				
Child	Atrophy	20	40	Whole
Adult	Fibrosis	60	80	Whole
Lymph nodes and lymphatics	Atrophy, sclerosis	50	70	Whole node
Large arteries and veins	Sclerosis	80	100	10 cm^2
Articular cartilage	None	500	5,000	Whole
Uterus	Necrosis, perforation	100	200	Whole
Vagina	Ulcer, fistula	90	100	Whole
Breast				
Child	No development	10	15	Whole
Adult	Atrophy, necrosis	50	100	Whole

Based on a combination of Rubin P, Casarett GW: Clinical Radiation Pathology, vol 1. Philadelphia, WB Saunders, 1968; and Emami et al., 1991, with permission.
Table compiled by Dr. Richard Miller. The figures in this table are a guide only.

Összefoglalás

- A normál szövetekben kialakuló sugárkárosodások megjelenési ideje és dózis-függése a proliferatív szerveződés függvénye
- A gyorsan megújuló szövetek hierarchikus szerveződésűek, a látencia idő nem függ a dózistól, a funkcionális sejtek életideje szabja meg. A gyógyulás ideje dózis-függő.
- A lassan megújuló szövetek szerveződése flexibilis, a károsodások megjelenési ideje dózis-függő.
- A károsodott szövetek a sejt-proliferáció felgyorsul
- A sugárkárosodások kialakulásában szerepet játszik a klonogén sejtek pusztulása, a késői mellékhatások szempontjából a beinduló citokin kaszkád is fontos.
- A strukturális szöveti tolerancia a celluláris sugárérzékenységtől függ, nem befolyásolja a besugárzott térfogat.
- A funkcionális tolerancia a szövet szervezeti felépítésétől függ, befolyásolja a besugárzott térfogat